Flexible and Printed Electronics

Extrusion printing of radio frequency coplanar waveguides with commercial dispensing equipment

Flexible and Printed Electronics

PAPER

Extrusion printing of radio frequency coplanar waveguides with commercial dispensing equipment

Nowab Reza Md Ashif[1,*], Ulrich Gengenbach[1], Pascal Maier[2,3], Alexander Kotz[2], Christian Koos[2,3] and Ingo Sieber[1]

[1] Institute for Automation and Applied Informatics, Karlsruhe Institute of Technology, Karlsruhe, Germany
[2] Institute of Photonics and Quantum Electronics, Karlsruhe Institute of Technology, Karlsruhe, Germany
[3] Institute of Microstructure Technology, Karlsruhe Institute of Technology, Karlsruhe, Germany
[*] Author to whom any correspondence should be addressed.

E-mail: nowab.ashif@kit.edu

Keywords: additive manufacturing, digital manufacturing, extrusion printing, coplanar waveguides, radio frequency

OPEN ACCESS

RECEIVED
7 October 2024

REVISED
13 March 2025

ACCEPTED FOR PUBLICATION
8 May 2025

PUBLISHED
19 May 2025

Abstract

Coplanar waveguides (CPWs) are fundamental components of radio frequency and microwave circuits used for a variety of applications in telecommunications, radar systems and wireless communications. There is a need for low-cost and easily accessible manufacturing techniques that enable the fabrication of CPWs using commercial materials and equipment, thus reducing production costs and facilitating easy access to these versatile transmission lines. In this paper, we present CPWs on alumina substrates fabricated with an extrusion printing process based on low-cost commercial dispensing equipment and a commercial silver ink. For a 4 mm long CPW, we observe an insertion loss below 1 dB and a return loss better than 10 dB for the frequency range from 40 MHz to 33.8 GHz.

1. Introduction

High speed optical data communication is the backbone of today's data-driven society and economy. It is based on fibre optic cables for signal transmission and photonic integrated circuits (PIC) for optical signal processing. While silicon photonics enables a high integration density, an integration challenge often arises when electro-optic devices (e.g. laser diodes) and electronics (e.g. drivers, amplifiers) have to be packaged with a silicon photonics chip.

Jacob *et al* outline four types of PIC integration strategies [1]:

In the hybrid integration strategy, the laser, the silicon photonics chip and the electronics chip are separately manufactured and subsequently packaged. In heterogeneous integration the laser and the silicon photonics chip are fabricated together (e.g. by III–V chiplet bonding) and the electronics chip is copackaged. Monolithic integration means that the photonics and electronics chips are fabricated together on the same wafer and the laser is copackaged. The highest and most challenging level is fully monolithic integration where all components are fabricated together and the subsequent packaging effort is minimised.

The hybrid integration strategy provides the highest flexibility, as the most mature process technologies can be selected for the respective subsystems (laser, silicon photonics, etc). The price for this flexibility is however an increased packaging effort based on multi-chip flip-chip packages or interposers. To date this is the integration strategy pursued in most silicon photonics foundries [1].

O'Brien *et al* [2] give an overview of PIC packaging technologies. With respect to electrical packaging they introduce ceramic interposers to fan out radio frequency (RF) transmission lines from photonic devices to larger pitched printed circuit boards (PCB) that ultimately terminate in RF connectors.

Ceramic materials have a high dielectric constant, which is advantageous for RF and microwave circuits. A higher dielectric constant allows for reduced dimensions of RF trans-mission lines and

components, leading to smaller and more compact designs [3]. Further, alumina demonstrates the ability to endure extreme temperatures and moisture and is also an inert and vacuum-compatible material [4].

To fan out RF transmission lines coplanar waveguides (CPWs) have the advantages over conventional microstrip lines that, due to high design freedoms, they are easier to realise for a desired line impedance [5], that they enable simple connection of external shunt elements (such as active components) as well as the creation of series and shunt capacitances [6], and show lower dispersion [7]. In addition, a size reduction of CPWs is possible without constraints, as the characteristic impedance depends only on the ratio between the width of the signal line and the distance between the signal and ground strips. Furthermore, the CPW line enables shunt elements to be grounded directly on the PCB trace. This configuration minimises crosstalk with neighbouring traces and offers lower losses in high-frequency applications compared to microstrip lines [8]. These advantages make CPWs ideal for use in integrated photonic circuits.

Thin-film technology is used to fabricate CPWs on the ceramic interposer that connect to the photonic device by through-substrate vias or wirebonds [9]. Mask based processes for RF waveguide fabrication on such interposers have low flexibility wrt design changes. Digital printing processes offer a flexible technological alternative for fabricating waveguides for photonic packaging.

A number of process chains based on digital printing processes have been proposed.

The aerosol jet printing (AJP) technology is used by both Chletsou *et al* [10] and He *et al* [11] to fabricate CPW transmission lines, but with different substrates and approaches. Chletsou *et al* use a low-viscosity silver nanoparticle (NP) ink, Metalon JS-A221AE, to print CPWs on acrylonitrile butadiene styrene (ABS) substrates for automotive applications. The ink is sintered using intense pulsed light (IPL) Sintering, achieving high-resolution CPWs with signal line widths as small as 300 μm and gaps between the signal and ground lines down to 25 μm. Line thicknesses of up to 14 μm are realized by multilayer printing. He *et al* fabricate CPWs on a single-crystalline diamond (SCD) substrate, utilizing silver NP ink and curing the printed lines at 150 °C for 40 min, followed by 200 °C for 20 min. The printed CPW is 2.44 mm long, fabricated on a 3.5 mm × 3.5 mm × 0.3 mm SCD substrate.

Inkjet printing is utilized in various processes by [12–14], each exploring its application in fabricating CPW transmission lines with different materials, substrates, and post-processing approaches. Kim *et al* [12] use silver NP ink on a glass substrate modified with a fluorocarbon film to create a high-resolution CPW with a gap of 15 μm, thickness over 2 μm, and a signal line width of 100 μm. Lee *et al* [13] print copper NP ink on a Bismaleimide–Triazine (BT) substrate, with a drop volume of 4 pL per dot, and achieve a metallic thickness of 5 μm after sintering. Sahu *et al* [14], on the other hand, fabricate CPWs on flexible polyethylene terephthalate substrates, using reel-to-reel inkjet printing of a copper NP ink as a precursor and for final waveguide fabrication by electroplating.

Microdispensing is also used in various processes for the fabrication of CPWs. Abdin *et al* [15] use an nScrypt 3Dn tabletop system to print the dielectric substrate with ABS filament, followed by micro-dispensing a 30 μm layer of silver paste. After thermal curing at 110 °C, IR laser structuring is applied to define the signal and ground line gaps, achieving precise dimensions for the CPW. The structural accuracy and RF properties in this process are primarily determined by the laser structuring rather than the printing process itself. In contrast, Rojas-Nastrucci *et al* [16] employs a different approach, where thick-film silver paste is micro-dispensed, and a picosecond Nd:YAG laser is used to solidify the edges, creating narrow gaps between the signal and ground lines (16–20 μm). This process focuses on enhancing precision in the slot formation, with the laser machining contributing significantly to the final structure. On the other hand, LeBlanc *et al* [17] explore a micro-dispensing process with silver NP ink, using polyether-ether-ketone (PEEK) as substrate. The addition of photonic curing enhances the electrical conductivity of the printed CPWs, improving their high-frequency performance.

Roemhild *et al* [18] use an XTPL Delta ultraprecision printer and a high viscosity silver NP ink (XTPL CL85) to fabricate CPWs on fused silica and Corning 1737 glass substrates by extrusion printing. The ink is sintered in an oven at 250 °C. The high precision of the printed waveguide is defined by the combination of a high viscosity ink, a printing nozzle with 5 μm orifice diameter and a high precision positioning system. The small line width achieved with the fine nozzle however requires to print many parallel overlapping lines to fabricate the CPW signal and ground conductors. This process yields a signal line width of 71.4 μm, gaps to the ground lines of 9.9 μm and 9.1 μm respectively but a line height of only 0.4 μm.

In this paper we introduce a low cost, straightforward extrusion printing process based on off-the-shelf dispensing equipment and a commercial high viscosity screen printing ink to fabricate CPWs. As the equipment used is already applied in electronic packaging, e.g. to dispense conductive adhesive, this process has the potential to be easily integrated into photonic packaging process chains. We investigate the RF performance of CPWs produced with this technique to assess the feasibility of this approach for high frequency applications. The low-cost approach introduced in this paper showcases the promise of

facilitating widespread CPW utilization and advancing innovation in high-frequency electronics.

The organisation of the paper is as follows: section 2 presents a brief introduction into the theory of CPWs. Section 3 shows results of extrusion printing experiments for determination of single line width. Section 4 covers design and simulation of the CPW structure. Section 5 shows optical inspection and electrical characterisation of printed CPWs. Section 6 deals with the discussion of the results and section 7 offers conclusions and an outlook.

2. Theory of CPWs

A traditional CPW structure on a dielectric substrate consists of a centre strip conductor (signal line) with semi-infinite ground planes on both sides, as shown in figure 1. This configuration supports a quasi-transverse electromagnetic (EM) mode of signal propagation.

Illustrated in figure 1 is a CPW featuring a signal line width (W), a gap between the signal line and ground line (W_g), a ground line width (GND), the substrate height (h), the printed structure height (t) the substrate/CPW length (L) and the relative permittivity of the substrate (ε_r).

The fields in CPW, and thus the EM energy, are almost equally divided between air and dielectric, especially when the gap is relatively small compared to the dielectric's thickness. This results in an effective relative permittivity for a CPW [19]:

$$\begin{aligned}\varepsilon_e &= \varepsilon_{r,e} \\ &= 0.5\,(\varepsilon_r+1)\,\{\tanh[1.785\log(h/Wg)+1.75] \\ &\quad + \left(\frac{kWg}{h}\right)[0.04-0.7k \\ &\quad +0.01\,(1-0.1\varepsilon_r)\,(0.25+k)]\}\end{aligned}$$

$$\text{Where} \qquad k=\frac{W}{W+2Wg} \qquad . \quad (1)$$

Equation (1) is accurate to 1.5% for $h/Wg \geqslant 1$ [20].

A good initial approach for analysis and design is to consider the effective permittivity as $(\varepsilon_r+1)/2$. The characteristic impedance of CPW is given by [6]:

$$Z_0 = \frac{30\pi}{\sqrt{\varepsilon_e}}\frac{K'(k)}{K(k)}$$

$$\text{Where} \qquad k' = \sqrt{(1-k^2)} \text{ and } K'(k) = K(k'). \qquad (2)$$

$K(k)$ and $K(k')$ are elliptic integrals. Using the ratio of the elliptic integrals allows the following simplifications [21]:

$$\frac{K(k)}{K'(k)} \approx \frac{1}{\pi}\ln\left(2\frac{1+\sqrt{k}}{1-\sqrt{k}}\right) \quad 0 \leqslant k \leqslant 0.707 \qquad (3)$$

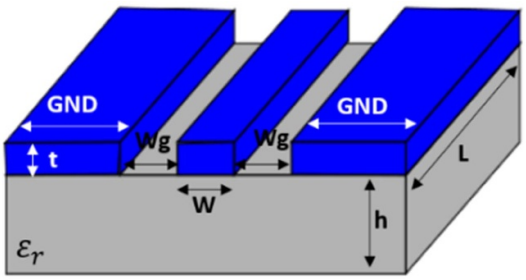

Figure 1. Coplanar waveguide.

$$\frac{K'(k)}{K(k)} \approx \frac{1}{\pi}\ln\left(2\frac{1+\sqrt{k'}}{1-\sqrt{k'}}\right) \quad 0.707 < k \leqslant 1. \qquad (4)$$

Equations (1)–(4) are for infinite ground CPW and used to calculate the gap width (W_g) between signal line and ground line for a CPW while the signal line width (W), substrate height (h), dielectric constant (ε_r) are known. The conductor thickness is ignored for this calculation. The calculation is performed with the aim of attaining a characteristic impedance of 50 ohms.

3. Determination of the single line width

In order to be able to position and move the dispensing equipment (cartridge and dispensing needle) for the dispensing trials with high precision, it is mounted on the numerically controlled, four-axis Cartesian handling platform MIMOSE [22] which was developed at our institute. For extrusion printing of the screen-printing ink Dyesol DYAG50 with solid content 75.5% to 85.0%, viscosity of 13 000–17 000 mPa· s, and resistivity of 5–6 $\mu\Omega$· cm we use the off-the-shelf dispensing needle Vieweg F561387-1/4 with 110 μm inner diameter. The DYAG50 conductive silver printing ink is comprised of a mixture of silver particles and an organometallic silver compound in an organic medium. The curing temperature of this ink is 160 °C–180°C. The fabrication process is carried out using a Nordson Ultimus-I dispenser on a pre-cleaned ceramic substrate. The ceramic substrate, Rubalit® 708 S with 96% Al_2O_3, has a thickness (h) of 500 μm, dielectric loss factor 0.01 and a dielectric constant (ε_r) of 8.3.

After systematic experimentation, we determine as optimal printing conditions a forward air pressure of 4.7 bar, a printing speed of 1 mm s^{-1}, and a needle stand-off distance of 70 μm [23].

The extrusion printing process occurs within an enclosed compartment, with continuous monitoring of humidity and temperature. After printing one line for running in the printing process, seven more lines (figure 2(a)) are printed to find out the average width of the printed lines. Printing a single line occurs in a top-to-bottom direction, while the progression

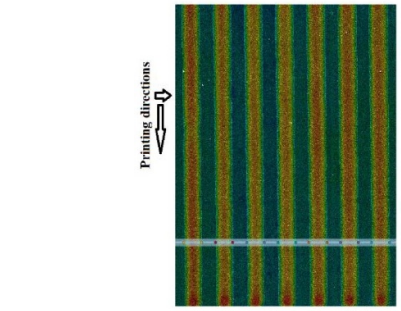

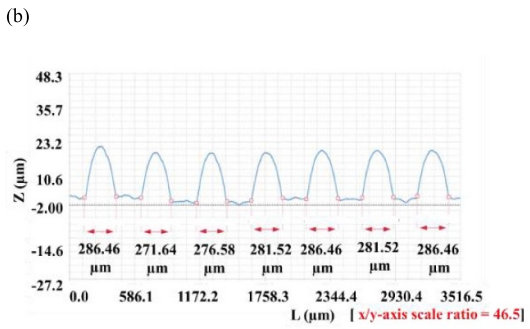

Figure 2. Profilometer measurement of line width.

for printing the next line moves from left to right (figure 2(a)). Subsequently the printed lines are subjected to a heating process in an oven at 170 °C for a duration of 10 min. This temperature treatment leads to the desired conductivity of the printed silver tracks.

Confocal optical measurements are performed using the Sensofar 3D optical profilometer S neox to determine the width of the printed structures. SensoVIEW software is used for data analysis. Figure 2 shows the optical measurement of the printed lines.

Figure 2 shows the optical measurement of the printed lines. In figure 2(a) dots of same colour indicate the measured distance between them and measurements are shown in figure 2(b) as a graph. For better representation we have used a different scale ratio in x and y axis in figure 2(b).

Table 1 presents the width variation, including the mean, standard deviation, and relative standard deviation for 20 points each (M1-M20) along the seven printed lines over a length of 5 mm.

By examining table 1, it is evident that the majority of the printed lines exhibit an average width ranging from 281 μm to 285 μm. The average line width is 281.97 μm.

The low standard deviation of the linewidth of a printed line illustrates the high reproducibility of this extrusion printing process with off-the-shelf commercial equipment.

This holds in particular as the time pressure dispenser controller applied in these experiments already has a specified pressure tolerance of $\pm$ 2% [24].

4. Design and simulation of the CPW structure

As the initial printing tests (see section 3) result in an average line width of the single line of 281.97 μm, a value of 282 μm is used for the design of the CPW as the signal line. With the target of an impedance of 50 ohms and the dielectric constant of our substrate $\varepsilon_r = 8.3$, the target gap width W_g is calculated to be 91 μm (equations (1)–(4)). The ground line width (GND) is chosen to be more than 2.5 times the width of the signal line (W). The printed line thickness is 20 μm. The EM-simulation is performed for a 4 mm long CPW using CST Studio Suite 2024. The time domain solver is used here, which can obtain the entire broadband frequency behaviour of the simulated device from a single calculation run.

The S-parameters, commonly referred to as scattering parameters, serve as crucial indicators for evaluating the signal transmission performance of a transmission line and depict the input-output relationships among ports within an electrical system, indicating the reflection and transmission characteristics in frequency domain [25]. For a CPW, S11 represents the input port voltage reflection coefficient, S22 represents the output port voltage reflection coefficient, S12 represents the reverse voltage gain, and S21 represents the forward voltage gain [26].

Figure 3 shows the simulation results, with the S11 and S22 parameters represented by blue circles and magenta dashed lines, and the S21 and S12 parameters represented by green squares and red dot-dashed lines, respectively. The S11 and S22 lines overlap due to the symmetry of the design and the uniformity of the line, and the same applies to the S21 and S12 lines.

Our initial target was to check the performance of our printed CPW up to 35 GHz. The above simulation results indicate that a CPW fabricated with these dimensions show good transmission properties in the range of 0–35 GHz.

5. Optical and electrical characterisation of the printed CPWs

Figure 4 illustrates a CPW printed on a ceramic substrate. The patterns we have printed exhibit continuous and straight edges with a stable boundary. Extrusion printing takes place from the right to the left. To achieve a wider ground line width, four parallel lines are printed, each spaced 150 μm apart to ensure effective overlap. The black marks on the structure are due to probe connection for RF measurements (see below). The image is taken with a Keyence VHX-770E Microscope.

Figure 5 displays the optical measurements obtained using the Sensofar 3D optical profilometer in confocal mode. These measurements are conducted to determine the height and width of the printed CPW structure.

Table 1. Width variation (mean, standard deviation and relative standard deviation) of printed lines.

Measurements	Line 1 (μm)	Line 2 (μm)	Line 3 (μm)	Line 4 (μm)	Line 5 (μm)	Line 6 (μm)	Line 7 (μm)
M1	279.54	274.46	303.5	294.82	294.82	294.82	303.5
M2	266.83	259.21	294.82	299.16	290.49	303.5	299.16
M3	277	261.75	290.49	281.82	286.15	299.16	290.49
M4	274.46	279.54	277.48	294.82	286.15	294.82	290.49
M5	284.62	271.92	286.15	281.82	281.82	299.16	294.82
M6	277	271.92	290.49	281.82	291.49	290.49	277.48
M7	289.71	277.00	281.82	273.15	286.15	290.49	277.48
M8	274.46	274.46	273.15	281.82	277.48	290.49	277.48
M9	282.08	261.75	286.15	286.15	290.49	286.15	290.49
M10	279.54	282.08	281.82	290.49	290.49	277.48	281.82
M11	292.25	279.54	277.48	277.48	286.15	286.15	286.15
M12	284.62	264.29	277.48	281.82	286.15	273.15	286.15
M13	284.62	271.92	286.15	281.82	277.48	273.15	286.15
M14	289.64	271.54	265.5	277.57	283.6	277.57	307.74
M15	297.33	274.46	268.81	277.48	281.82	273.15	273.15
M16	286.46	271.64	276.58	281.52	286.46	281.52	286.46
M17	292.25	274.46	273.15	277.48	277.48	273.15	268.81
M18	287.16	284.62	281.82	268.81	277.48	273.15	281.82
M19	289.71	287.16	273.15	268.81	277.48	268.81	273.15
M20	284.62	277.00	273.15	281.82	281.82	273.15	268.48
Average (μm)	283.69	273.53	280.95	282.02	284.57	283.97	285.06
Standard deviation (μm)	7.41	7.48	9.32	8.01	5.37	10.84	10.90
Relative standard deviation (%)	2.61	2.73	3.31	2.84	1.88	3.81	3.87

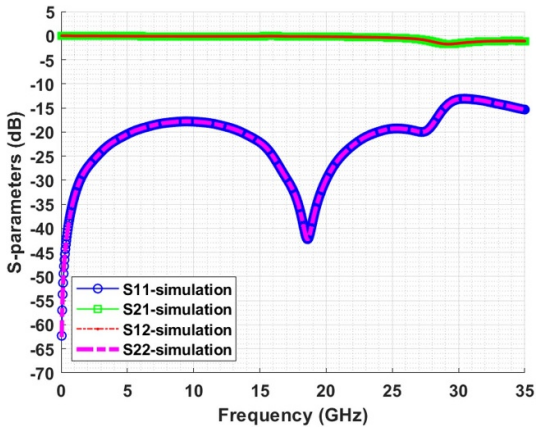

Figure 3. Simulation results.

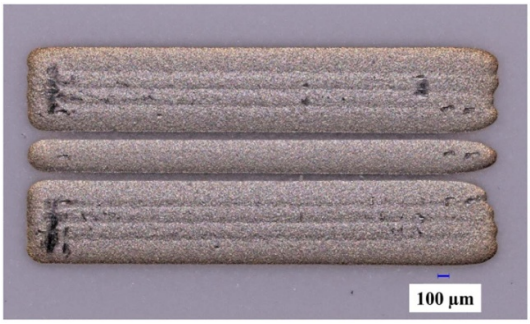

Figure 4. Printed CPW on ceramic substrate (top view).

In modelling the CPW structures, rectangular line profiles are used. However, such rectangular structures cannot be produced by the extrusion printing process, resulting in rounded edges (see figure 5(b)). The CPW is designed to have a gap (W_g) of 91 μm between signal and ground line on both sides. However, the profile measurements illustrate that due to process tolerances we are unable to achieve the same gap on both sides of the signal line (see figure 5).

Table 2 showcases the measurements of ground line widths (GND 1 and GND 2), gaps (Gap 1 and Gap 2), along with signal line width and height. These measurements are at 16 distinct points along a 4 mm length of the CPW.

The relative standard deviations of the dimensions deviations observed are below 2.53% for the printed lines and below 8.54% for the gaps. This can be attributed to the printing tolerances identified above. These results again validate the high reproducibility of the extrusion printing process and thus its suitability for fabrication of RF waveguides.

For assessing the S-parameters of this CPW, we used the Anritsu 37 397 C vector network analyser (VNA) covering a frequency range from 40 MHz to 35 GHz. VNA coaxial cables are connected to the MPI T67A GSG400 ground-signal-ground RF probe,

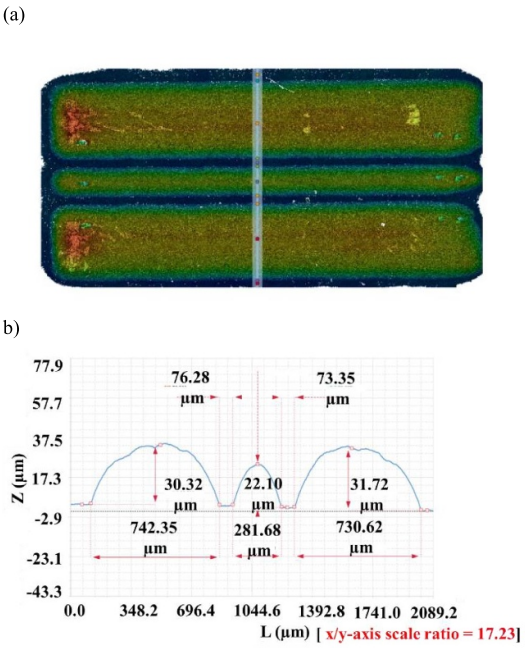

Figure 5. Profilometer measurement of CPW (a) top view (b) width and height measurement.

Table 2. Measurements of ground line widths, gaps, signal line width and signal line height.

Measure-ments	GND1 (μm)	GAP 1 (μm)	Signal line width (μm)	GAP 2 (μm)	GND2 (μm)	Signal line height (μm)
M1	762.82	65.88	291.11	59.75	746.26	21.27
M2	752.71	66.74	291.06	63.03	745.99	21.02
M3	752.4	65.76	292.5	64.57	742.06	22.36
M4	755.39	68.67	283.64	76.58	740.81	22.31
M5	749.42	62.7	301.56	65.68	743.44	20.96
M6	740.46	74.64	280.66	71.65	719.56	21.16
M7	746.43	77.62	280.66	77.62	736.53	21.68
M8	743.44	74.64	286.63	68.67	731.5	21.59
M9	742.35	76.28	281.68	73.35	730.62	22.10
M10	734.49	80.61	280.66	74.64	734.49	21.81
M11	746.66	74.66	280.74	77.65	737.7	21.50
M12	749.42	80.61	274.69	77.62	728.52	21.91
M13	734.49	80.61	280.66	71.65	728.52	21.04
M14	746.6	77.65	280.74	71.67	722.77	20.48
M15	737.7	77.65	283.73	77.65	731.73	22.23
M16	740.69	77.65	274.77	80.63	725.75	21.80
Average (μm)	745.96	73.9	284.09	72.03	734.14	21.57
Standard deviation (μm)	7.72	5.96	6.98	6.15	8.16	0.54
Relative standard deviation (%)	1.03	8.06	2.45	8.54	1.11	2.53

which has a pitch size of 400 μm, to connect both ends of the CPW.

The calibration is carried out utilizing the AC5 calibration substrate (GSG-GS-SG). In this calibration process, the SOLT(Short-open-load-through) method is applied, ensuring precise calibration up to the extremity of the RF probe. Figure 6 displays measured results by VNA, with S11 and S22 parameters represented by red dash and green dot lines(see figure 6(a)), and S21 and S12 parameters represented by red dash and green dot lines(see figure 6(b)), respectively. S11 and S22 curves do not completely overlap because of non-uniformity of the line. The same goes for S21 and S12.

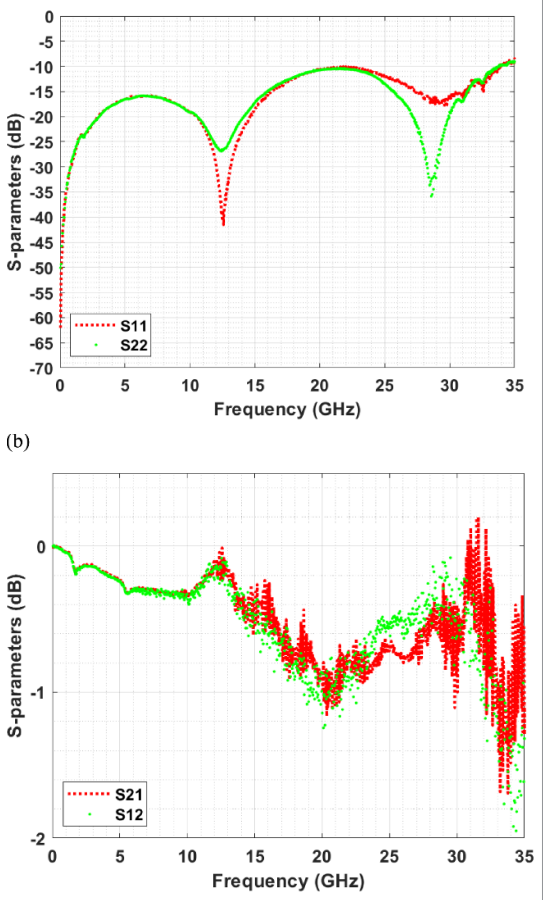

Figure 6. Measured return loss and insertion loss of CPW (a) return loss, S11, S22 (b) insertion loss, S21, S12.

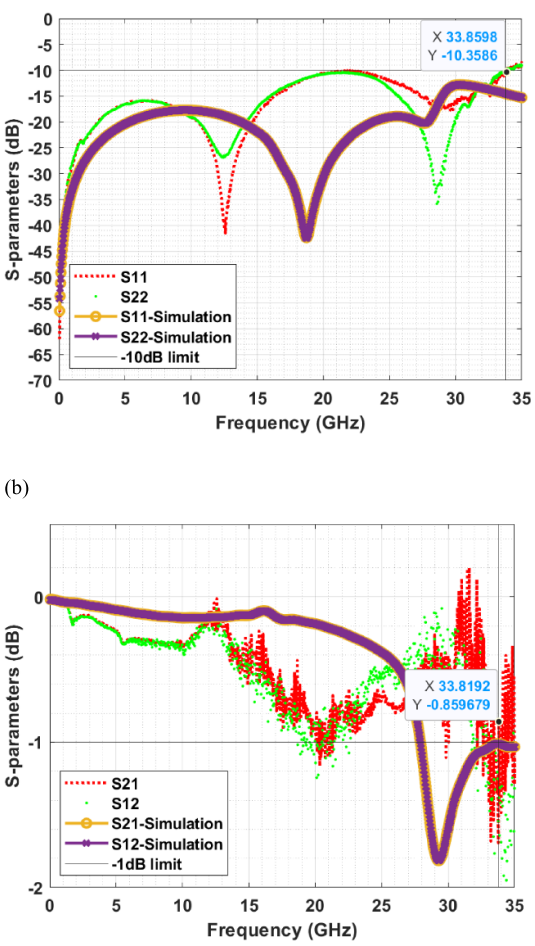

Figure 7. Measured and simulated insertion loss and return loss of CPW (a) return loss, S11, S22 (b) insertion loss, S21, S12.

6. Results and discussion

We have achieved a linewidth of the printed lines with a low standard deviation, which illustrates the high reproducibility of this extrusion printing process with off-the-shelf commercial equipment. The characteristic impedance of the CPW lines mainly depends on the signal line width and the gap to the ground line. Variations in the signal line width and in the gap along the line cause impedance variation which results in more reflections along the line [27]. The characteristic impedance for the printed CPW depicted in figure 4 is 46.9 ohms, determined with the equations (1)–(4) using average values of the geometrical parameters presented in table 2.

The deviation from the 50 ohms characteristic impedance is due to differences in signal line width and gap between designed (see section 4) and printed CPW (see section 5).

Figure 7 demonstrates the comparison between measured S-parameters and simulated S-parameters (for averaged parameters from table 2). Figure 7(a) shows the S11 and S22 in dB vs frequency in GHz and figure 7(b) shows the S21 and S12 in dB vs frequency in GHz. In figures 7(a) and (b) a shift between measurements and simulations is observable.

The reason for this shift is, because the printed signal and ground lines exhibit non-uniform width along their length, accompanied by a significant variation in the gap dimensions along the entire span (see table 2) and also a non-rectangular shape of the printed lines. Using a CAD representation based on measurement data of manufactured CPWs in modelling will help to create a geometrical representation that more closely matches the printed structures. This will reduce the deviation between measured and simulated results. The substrate loss and material loss also contribute to the deviation between the measured and simulated results.

Another reason for the variation in the curves of S11 and S22 in the measured S-parameters arises from the asymmetry in the transmission line, attributed to tolerances of the printing process [28].

The measurements of the 4 mm CPW sample show a good RF performance up to 33.8 GHz, where insertion loss is less than or close to 1 dB, while return loss is better than 10 dB. The peak value of S21 is close to 0 dB. From figure 7, it is evident that at frequencies of 10 GHz and 33.8 GHz, the measured S21 values

Table 3. Comparison with other printed CPWs.

Paper	Insertion loss (dB mm^{-1}) @ 10 GHz	Insertion loss (dB mm^{-1}) @ 33.8 GHz	Process steps	Dimen-sions ($W/W_g/t$) (μm)	Sub-strate	Ink
This work	0.08	0.21	1) DP-SP 2) TS	281/74/22	Ceramic	Ag NP paste
[11]	0.075	0.175	1) AJP-MP 2) TS	217/70/3	SCD	Ag NP ink
[10]	0.24	0.52	1) AJP-MP 2) IPL sintering	300/25/12	ABS	Ag NP ink
[12]	0.2	0.42	1) Photo-lithography 2) IP-MP 3) TS	100/15/2	Glass wafer	Ag NP ink
[13]	0.14	NA	1) IP 3) TS	25/75/5	BT	Cu NP ink
[17]	0.075	0.25	1) DP 2) TS	550/150/NA	PEEK	Ag paste

(TS = Thermal sintering, BT = Bismaleimide-Triazine, IP = Inkjet printing, IPL = Intense Pulse Light, DP = Dispensing, NP = Nanoparticle, PEEK = Poly-ether-ether-ketone, SCD= Single crystal diamond, MP= Multi pass, SP = Single pass).

are −0.32 dB and −0.85 dB, resulting in an observed average loss per millimeter of 0.08 dB mm^{-1} and 0.21 dB mm^{-1}, respectively. In comparison, the simulated S21 values at these frequencies are −0.14 dB and −1.01 dB, leading to simulated average loss values of 0.035 dB mm^{-1} and 0.25 dB mm^{-1}, respectively. The difference between the simulated and measured average loss per millimeter at these two frequencies is 0.045 dB mm^{-1} and 0.04 dB mm^{-1}.

Table 3 compares this work with CPWs manufactured with different processes, different inks on different substrates from the literature. Due to limited data availability, some of the insertion loss values are approximate, extracted from graphs provided in the literature. The insertion loss values in this work (0.08 dB mm^{-1} at 10 GHz and 0.21 dB mm^{-1} at 33.8 GHz) are close to some of the referenced works, particularly [11] and [17]. At 10 GHz, this work outperforms the results of [10, 12] and [13]. At 33.8 GHz, this work (0.21 dB mm^{-1}) surpasses the results of [10] and [12].

Additionally, the single-pass dispensing method used in this work, combined with thermal sintering, offers a simple and fast process compared to more complex process chains, such as AJP and inkjet printing [10, 11, 13] and even photolithography [12].

The focus of this work is on the application of readily available, commercial equipment in the fabrication of CPWs. This achieves high-cost efficiency and process simplicity, enabling competitive performance at both 10 GHz and 33.8 GHz. The ultra-high resolution and precision, which are sometimes achieved by complex high precision multi-pass printing or photolithography methods, are not attained by the presented method.

7. Conclusions and outlook

System integration of PICs requires fabrication of RF waveguides ranging from millimeter scale connectors to transmission lines several hundred micrometers wide to interface a silicon photonics chip. The main objective of this study is to evaluate the potential of extrusion printing with off-the-shelf dispensing equipment on an alumina substrate using conductive silver screen printing ink for fabrication of CPW RF transmission lines. Initial extrusion printing tests indicated that lines with a width of about 280 μm can be reproducibly printed with good edge quality. This dimension was used as signal line width for designing a CPW by means of modelling and simulation. The simulation yielded a CPW design with good transmission performance up to about 35 GHz. This design was printed with the extrusion printing process and dimensionally and electrically characterised. The dimensional characterisation showed low tolerances with respect to signal line width and signal to ground line gap width which is an indication of the

high reproducibility of the extrusion printing process. The electrical characterisation of the printed samples showed good RF transmission up to 33.8 GHz, which is in good agreement with the simulation results.

The comparison of insertion loss values with other works from literature also shows that extrusion printing with off-the-shelf dispensing equipment is suitable as a cost-effective additive digital manufacturing process for RF transmission lines. The next steps involve optimizing the process and equipment for CPWs designed for higher frequencies by using dispenser needles with smaller diameters in combination with lower viscosity paste and substrates with better surface quality. Moreover, it is also worth investigating whether it will be possible to print on different substrates without significant degradation of the shape and RF properties of the printed CPWs.

Furthermore, a more realistic CAD model of the printed CPW based on measurement data will be implemented for simulation, aiming to obtain results that more closely match the measured data and thus allow a model-based waveguide and fabrication process design.

Data availability statement

All data that support the findings of this study are included within the article (and any supplementary files).

Acknowledgments

This work was supported by the program Materials Systems Engineering of the Helmholtz Association, by the Deutsche Forschungsgemeinschaft (DFG, German Research Foundation) via the Excellence Cluster 3D Matter Made to Order (EXC-2082/1–390761711), by the ERC Consolidator Grant TeraSHAPE (# 773248), by the BMBF project Open6GHub (# 16KISK010), and by the Karlsruhe School of Optics & Photonics (KSOP).

ORCID iDs

Nowab Reza Md Ashif https://orcid.org/0009-0001-7551-6728
Pascal Maier https://orcid.org/0000-0002-6655-6592
Ingo Sieber https://orcid.org/0000-0003-2811-7852

References

[1] Jacob A P, Chandran S, Van Campenhout J, Pantouvaki M, Heck J, Giewont K, Rakowski M, Bian Y, Debackere P and Kuntz M 2023 Photonic integrated circuit fabrication and test approaches *Integrated Photonics for Data Communication Applications* ed M Glick *et al* (Elsevier) ch 11, pp 368–410
[2] O'Brien P, Gradkowski K, Morrissey P E, Latkowski S, Gehring H, Pernice W and Smolenski J 2023 Packaging and test technologies *Integrated Photonics for Data Communication Applications* ed M Glick *et al* (Elsevier) ch 12, pp 411–38
[3] Ullah M H and Islam M T 2012 Design of a modified W-shaped patch antenna on Al_2O_3 ceramic material substrate for Ku-band *Chalcogenide Lett.* **9** 61–6
[4] Uttiya S, Bernini C, Vignolo M, Pallecchi I, Marré D, Siri A S and Pellegrino L 2017 Inkjet printing of conducting silver patterns on alumina and insulating ceramic-glass by saline precursors *Thin Solid Films* **642** 370–6
[5] Simons R N 2004 *Coplanar Waveguide Circuits, Components, and Systems* (Wiley) p 1
[6] Wen C P 1969 Coplanar waveguide: a surface strip transmission line suitable for nonreciprocal gyromagnetic device applications *IEEE Trans. Microw. Theory Tech.* **17** 1087–90
[7] Deal W R 2008 Coplanar waveguide basics for MMIC and PCB design *IEEE Microw. Mag.* **9** 120–33
[8] Mahajan R C, Parashar V, Vyas V and Sutaone M 2019 Design and implementation of defected ground surface with modified co-planar waveguide transmission line *SN Appl. Sci.* **1** 1–12
[9] Zwickel H, Kemal J N, Kieninger C, Kutuvantavida Y, Rittershofer J, Lauermann M, Freude W, Randel S and Koos C 2018 Electrically packaged silicon-organic hybrid (SOH) I/Q-modulator for 64 GBd operation *Opt. Express* **26** 34580–91
[10] Chletsou A, Bannon A, Konstantinou X, Reimnitz L, Locke J and Papapolymerou J 2022 Additive manufactured CPW lines cured by intense pulse light for automotive microwave applications *2022 52nd European Microwave Conf. (Eumc)* (IEEE) pp 377–80
[11] He Y, Becker M, Grotjohn T, Hardy A, Muehle M, Schuelke T and Papapolymerou J 2017 RF characterization of coplanar waveguide (CPW) transmission lines on single-crystalline diamond platform for integrated high power RF electronic systems *2017 IEEE MTT-S Int. Microwave Symp. (IMS)* (IEEE) pp 517–20
[12] Kim H, Yun G Y, Lee S H and Kim J M 2015 High-resolution CPW fabricated by silver inkjet printing on selectively treated substrate *Sens. Actuators A* **224** 1–5
[13] Lee H J, Seo S, Yun K, Joung J W, Oh I Y and Yook J G 2008 RF performance of CPW transmission line fabricated with inkjet printing technology *2008 Asia-Pacific Microwave Conf.* (IEEE) pp 1–4
[14] Sahu A, Devabhaktuni V, Lewandowski A, Barmuta P, Wallis T M, Shkunov M and Aaen P H 2015 Microwave characterization of ink-jet printed CPW on PET substrates *2015 86th ARFTG Microwave Measurement Conf.* (IEEE) pp 1–4
[15] Abdin M M, Johnson W J D, Wang J and Weller T M 2019 W-band finite ground coplanar waveguide (FG-CPW) using laser enhanced direct-print additive manufacturing (LE-DPAM) *2019 IEEE MTT-S Int. Microwave Symp. (IMS)* (IEEE) pp 1213–6
[16] Rojas-Nastrucci E A, Tsang H, Deffenbaugh P I, Ramirez R A, Hawatmeh D, Ross A and Weller T M 2017 Characterization and modeling of K-band coplanar waveguides digitally manufactured using pulsed picosecond laser machining of thick-film conductive paste *IEEE Trans. Microw. Theory Tech.* **65** 3180–7
[17] LeBlanc S, Church K and Rojas-Nastrucci E A 2021 Photonic curing of mm-wave coplanar waveguides for conductor loss enhancement *2021 IEEE 21st Annual Wireless and Microwave Technology Conf. (WAMICON)* (IEEE) pp 1–3
[18] Roemhild M, Gramlich G, Baur H, Zwick T and Fruehauf N 2023 Ultraprecise printing of $ D $-band transmission lines *IEEE Microw. Wirel. Technol. Lett.* **33** 1419–22
[19] Hilberg W 1969 From approximations to exact relations for characteristic impedances *IEEE Trans. Microw. Theory Tech.* **17** 259–65
[20] Steer M 2019 Microwave and RF design, volume 3: networks p 156 9781469656946

[21] Houdart M 1976 Coplanar lines: application to broadband microwave integrated circuits *1976 6th European Microwave Conf.* (IEEE) pp 49–53
[22] Gengenbach U K 1996 Automatic assembly of micro-optical components *Proc. SPIE* **2906** 141–50
[23] Ashif N R M D, Gengenbach U and Sieber I 2024 Process development for digital fabrication of radio frequency transmission lines with off-the-shelf equipment *2024 Symp. on Design, Test, Integration and Packaging of MEMS/MOEMS (DTIP)* (*Dresden, Germany*) pp 1–5
[24] Ungerer M, Debatin C, Martel J, Maurer V, Reichert K M, Hofmann A and Gengenbach U 2024 A reproducible extrusion printing process with highly viscous nanoparticle inks *Eng. Res. Express* **6** 015042
[25] Horn A F, Reynolds J W and Rautio J C 2010 Conductor profile effects on the propagation constant of microstrip transmission lines *2010 IEEE MTT-S Int. Microwave Symp.* (*Anaheim, CA, USA*) pp 868–71
[26] Chiang Y-C, Tseng H-W, Yu C-J, Lee C-Y, Huang C-C and Ho C-E 2023 High-frequency signal transmission in a coplanar waveguide structure with different surface finishes *Thin Solid Films* **784** 140079
[27] Amoli N A, Sivapurapu S, Chen R, Zhou Y, Bellaredj M L, Kohl P A, Sitaraman S K and Swaminathan M 2019. Screen-printed flexible coplanar waveguide transmission lines: multi-physics modeling and measurement *2019 IEEE 69th Electronic Components and Technology Conf. (ECTC)* (IEEE) pp 249–57
[28] Shi Y, Jiang Z, Lam S, Leach M, Wang J and Lim E G 2017 Multi-GHz microstrip transmission lines realised by screen printing on flexible substrates*2017 IEEE Electrical Design of Advanced Packaging and Systems Symp. (EDAPS)* (IEEE) pp 1–3